Powerful Templating Effect in Rb/Pd/Se_x Promoted by Crown Ether-like $[Rb(Se_8)]^+$ Coordination. Formation of $Rb_2[Pd(Se_4)_2]\cdot Se_8$: A Layered Pd Polyselenide with "Encapsulated" Eight-Membered Selenium Rings

Michael Wachhold and Mercouri G. Kanatzidis*

Contribution from the Department of Chemistry and Center for Fundamental Materials Research, Michigan State University, East Lansing, Michigan 48824

Received November 23, 1998

Abstract: A novel layered Rb−Pd polyselenide has been synthesized by methanothermal reaction of Pd^{2+} with Se_x^{2-} (from Se^{2-} + Se) in the presence of Rb_2CO_3. $Rb_2[Pd(Se_4)_2]\cdot Se_8$ (**I**) reveals a unique structure with infinite $[Pd(Se_4)_2]^{2-}$ sheet polyanions acting as a host for neutral Se_8 rings. The black shiny rectangular crystals of $Rb_2[Pd(Se_4)_2]\cdot Se_8$ are insoluble in H_2O and common organic solvents. The compound crystallizes in the noncentrosymmetric space group $P\bar{4}b2$ (No. 117) with $a = 12.6748(8)$ Å, $c = 6.9273(7)$ Å, $Z = 2$, and $V = 1112.9(2)$ Å^3. The $[Pd(Se_4)_2]^{2-}$ sheet anion contains Pd^{2+} ions with a distorted square planar coordination geometry to four terminal Se atoms of Se_4^{2-} chains. The cocrystallized neutral Se_8 rings have a crown-like conformation as known from the elemental Se_8 forms. Through coordination to Rb^+ ions they build $[Rb(Se_8)^+]_n$ "cationic chains" running in the *c* direction. $Rb_2[Pd(Se_4)_2]\cdot Se_8$ therefore differs fundamentally from its "neighboring" alkali metal Pd polyselenides, K_2PdSe_{10} and Cs_2PdSe_8, which each possess a three-dimensional structure with two interpenetrating $[Pd(Se_x)_2]^{2-}$ frameworks. Optical spectroscopic data and the thermal stability of the compound are discussed.

Introduction

In recent years solventothermal synthesis methods have been successfully used for the preparation of numerous novel Main Group and transition metal chalcogenides.[1] A very important factor regarding the formation of such compounds is the structure-directing effect of different cations with various sizes and shapes. The effect is well-known in zeolite and other microporous compounds,[2] although in exactly what way the counterion directs the structure of the anionic frameworks has not been articulated. We have made the first steps beyond merely identifying that the effect exists and toward describing more exact cation size/anionic structure relationships associated with this effect as it applies to chalcogenide and polychalcogenide chemistry and by implication to other types of materials.[3] In this respect the Pd polyselenide system is interesting because it is highly responsive to changes in countercations. For example, $K_4[Pd(Se_4)_2][Pd(Se_6)_2]$ (=K_2PdSe_{10}),[4] $Cs_2[Pd(Se_4)_2]$ (=Cs_2PdSe_8),[5] $K_2(enH_2)_2[Pd(Se_4)_2\cdot 2Se_4]$,[6] $\{(CH_3)N(CH_2CH_2)_3N\}_2[Pd(Se_6)_2]$,[6] $(enH)_2[Pd(Se_5)_2]$,[6] $(NEt_4)_5[Pd(Se_4)_2\cdot 0.5Pd(Se_5)_2]$,[7] and $(Ph_4P)_2[Pd(Se_4)_2]$[8] all contain $[Pd(Se_x)_2]$ frameworks which feature different architectures. The structural analysis of all compounds clearly shows a trend to form lower-dimensional structures with an increasing cation size, while the Pd atom always maintains a square-planar geometry. Whereas $K_4[Pd(Se_4)_2][Pd(Se_6)_2]$, $Cs_2[Pd(Se_4)_2]$, and $K_2(enH_2)_2[Pd(Se_4)_2\cdot 2Se_4]$ all reveal three-dimensional (3D) frameworks, $\{(CH_3)N(CH_2CH_2)_3N\}_2[Pd(Se_6)_2]$ and $(enH)_2[Pd(Se_5)_2]$ show sheetlike, two-dimensional (2D) Pd polyselenide anions. Due to the large Ph_4P^+ and Et_4N^+ cations, $(Ph_4P)_2[Pd(Se_4)_2]$[8] and $(NEt_4)_5[Pd(Se_4)_2\cdot 0.5Pd(Se_5)_2]$[7] possess discrete $[Pd(Se_4)_2]^{2-}$ anions, in which each Pd^{2+} is coordinated by two chelating Se_4^{2-}-ligands. In the reaction of K_2PdCl_4 and K_2Se_5 in a 1:6 ratio, the high concentration of both polyselenide anions and potassium cations forces the formation of the highly charged, isolated $[Pd(Se_5)_4]^{6-}$ anion in $K_6[Pd(Se_5)_4]$. It has been discussed as the possible precursor species for the formation of 2D or 3D polyselenides.[6]

Remarkably, both K_2PdSe_{10} and Cs_2PdSe_8 display interpenetrating 3D frameworks. The K^+ salt consists of two different frameworks, i.e., $[Pd(Se_4)_2]^{2-}$ and $[Pd(Se_6)_2]^{2-}$ polyanions, whereas the Cs^+ salt reveals two frameworks with the same stoichiometry of the former polyanion. Both compounds adopt diamond-like arrangement, topologically equivalent to the structure of crystobalite SiO_2,[9] where the Pd^{2+} ions occupy the Si sites and the Se_x^{2-} ligands the O sites.

(1) (a) Sheldrick, W. S.; Wachhold, M. *Angew. Chem., Int. Ed. Engl.* **1997**, *36*, 206. (b) Kanatzidis, M. G.; Huang, S.-P. *Coord. Chem. Rev.* **1994**, *130*, 509. (c) Drake, G. W.; Kolis, J. W. *Coord. Chem. Rev.* **1994**, *137*, 131. (d) Bowes, C. L.; Ozin, G. A. *Adv. Mater.* **1996**, *8*, 13. (e) Sheldrick, W. S.; Wachhold, M. *Coord. Chem. Rev.* **1998**, *176*, 211.

(2) (a) Davis, M. E. *CHEMTECH* **1994**, *24*, 22. (b) Lewis, D. W.; Sankar, G.; Wyles, J.; Thomas, J. M.; Catlow, C. R. A.; Willock, D. J. *Angew. Chem., Int. Ed. Engl.* **1997**, *36*, 2675. (c) Oliver, S.; Kuperman, A.; Ozin, G. A. *Angew. Chem., Int. Ed. Engl.* **1998**, *37*, 46.

(3) (a) Kanatzidis, M. G. *Phosphorus, Sulfur Silicon Relat. Elem.* **1994**, *93*−*94*, 159. (b) Huang, S. P.; Kanatzidis, M. G. *Inorg. Chem.* **1991**, *30*, 1455.

(4) Kim, K.-W.; Kanatzidis, M. G. *J. Am. Chem. Soc.* **1992**, *114*, 4878.

(5) Li, J.; Chen, Z.; Wang, R.-J.; Lu, J. Y. *J. Solid State Chem.* **1998**, *140*, 149.

(6) Kim, K.-W.; Kanatzidis, M. G. *J. Am. Chem. Soc.* **1998**, *120*, 8124.

(7) McConnachie, J. M.; Ansari, M. A.; Ibers, J. A. *Inorg. Chem.* **1993**, *32*, 3250.

(8) (a) Kräuter, G.; Dehnicke, K. *Chem. Ztg.* **1990**, *114*, 7. (b) Ansari, M. A.; Mahler, C. H.; Chorghade, G. S.; Lu, Y.-J.; Ibers, J. A. *Inorg. Chem.* **1990**, *29*, 3832. (c) Adams, R. D.; Wolfe, T. A.; Eichhorn, B. W.; Haushalter, R. C. *Polyhedron* **1989**, *8*, 701.

10.1021/ja984053g CCC: $18.00
Published on Web 04/14/1999

In K_2PdSe_{10} the existence of two different ligands Se_4^{2-} and Se_6^{2-} in the independent frameworks presumably originates from the tendency to pack optimally around the K cation. In the Cs^+ compound the Se_6^{2-} chain has been formally substituted with a Se_4^{2-} chain helping to generate the needed space for the larger cation. Another noteworthy compound is $(NH_4)_2[PdS_{11}]$,[10] but the disorder of the sulfur chains precludes one from unequivocally deciding whether the compound is layered or three-dimensional.

We considered it worthwhile to characterize a Rb−Pd polyselenide, since the diameter of Rb^+ (1.66 Å, for 6-fold coordination) lies between those of K^+ (1.52 Å) and Cs^+ (1.81 Å).[11] One could expect a similar construction of two interpenetrating frameworks with assigned Se_x^{2-} chains. As a result we report the synthesis and structural and physical characterization of $Rb_2[Pd(Se_4)_2]\cdot Se_8$ (**I**), which reveals an unexpected sheetlike polyanion $[Pd(Se_4)_2]^{2-}$ with "intercalated" crown-like Se_8 eight-membered rings. To the best of our knowledge, this compound represents the first example of cocrystallized Se_8 molecules. It also represents a prominent example of a template-induced compound formation in which an otherwise very stable alternative (i.e. Rb_2PdSe_8 or Rb_2PdSe_{10}) is circumvented in favor of a completely unanticipated, but apparently even more stable selection of $Rb_2[Pd(Se_4)_2]\cdot Se_8$.

Results and Discussion

Structure. The successful isolation of $Rb_2[Pd(Se_4)_2]\cdot Se_8$ fills a gap in the series of alkali metal Pd polyselenide A−Pd−Se compounds with A = K, Rb, Cs. The close structural relationship of K_2PdSe_{10} and Cs_2PdSe_8 leads to the expectation of a similar buildup of interpenetrating $[Pd(Se_x)_2]$ framework for Rb^+, as it is present in these two compounds, with appropriate adjustments to accommodate the Rb^+ cations, if necessary.

From this point of view, the isolation and structure of $Rb_2[Pd(Se_4)_2]\cdot Se_8$ is a rather surprising result. We now find a two-dimensional sheetlike polyanion $[Pd(Se_4)_2]^{2-}$ (Figure 1), lying within the tetragonal plane, rather than a three-dimensional framework structure. The main reason for the lowering of dimensionality for the $[Pd(Se_4)_2]^{2-}$ unit is the adoption of voluminous Se_8 rings as guest molecules between the sheets. Therefore this compound can be described as a host−guest type of structure. The counterions in this compound then are thought to be the crown ether-like $[Rb(Se_8)^+]$ fragments.

In the 2D $[Pd(Se_4)_2]^{2-}$ anion, the Pd^{2+} ions lie on a special position (0/0/0) and therefore are all in one plane. Each Pd^{2+} center is coordinated by four Se_4^{2-} chains in a distorted square-planar coordination environment. Each Se_4^{2-} chain bridges two Pd^{2+} centers. The Pd−Se(1) distances of 2.4339(6) Å lie on the lower end of the values observed so far in the other known polyselenides (range 2.438−2.468 Å). The distortion of the square-planar $PdSe_4$ unit, toward a tetrahedral arrangement, is rather high in this compound (Figure 2a) and not observed in other polyselenides; the Se(1)−Pd-Se(1) angles are 90.495(3)° for cis and 169.34(3)° for trans Se atoms, respectively. Therefore, the four Se(1) atoms are 0.226 Å away from the least-squares plane through this $Pd(Se)_4$ unit.

The bond lengths and angles in the Se_4^{2-} chains lie within the expected range (Table 3) and are similar to values observed in other Se_x^{2-} chains of known Pd polyselenides.[4−8] The Pd−Se(1)−Se(2) angle with 106.31(3)° is slightly higher than the Se−Se−Se angles within the chain.

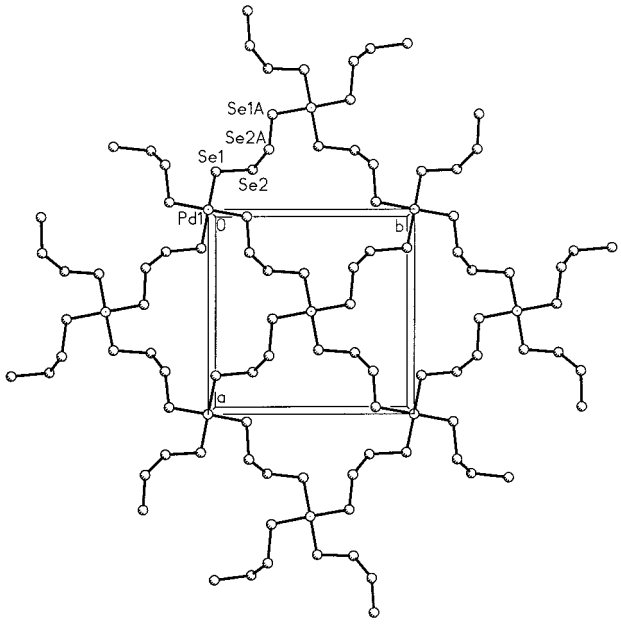

Figure 1. Structure of the 2D $[Pd(Se_4)_2]^{2-}$ polyanion in $Rb_2[Pd(Se_4)_2]\cdot Se_8$.

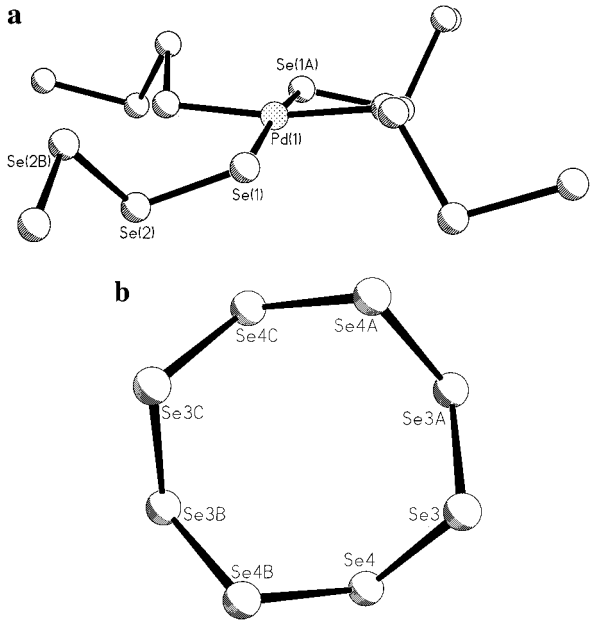

Figure 2. (a) The distorted square-planar $Pd(Se_4)$ fragment of the $PdSe_{16}$ building block of the 2D $[Pd(Se_4)_2]^{2-}$ sheet; the Se(1)−Pd−Se(1) angle between the trans Se atoms is 169.34(3)°, and the Se(1) atoms reveal a distance of 0.226 Å from the least-squares plane through the Pd ion. (b) Neutral Se_8 rings in $Rb_2[Pd(Se_4)_2]\cdot Se_8$, viewed from the [100] direction; they reveal a crown conformation known from the elemental Se_8 forms.

The Se_8 rings show the same crown-like conformation (Figure 2b) found in the elemental α-, β-, or γ-Se_8 forms.[12] Within the crystal structure this molecule departs from its ideal D_{4d} symmetry and adopts a D_2 symmetry. The Se−Se distances range from 2.364(2) to 2.379(2) Å, which is slightly higher than the values observed in the elemental forms (2.334(5) Å). The coordination to the alkali metal, which is evident in the structure,

(9) Greenwood, N. N.; Earnshaw, A. *Chemistry of the Elements*, 1st ed.; Pergamon: Oxford, 1990; p 393.
(10) Haradem, P. S.; Cronin, J. L.; Krause, R. A.; Katz, L. *Inorg. Chim. Acta* **1977**, *25*, 173.
(11) Shannon, R. D. *Acta Crystallogr. A* **1976**, *32*, 751.
(12) (a) Cherin, P.; Unger, P. *Acta Crystallogr. B* **1972**, *28*, 313. (b) Marsh, R. E.; Pauling, L.; McCullough, J. D. *Acta Crystallogr.* **1953**, *6*, 71. (c) Voss, O.; Janickis, V. *J. Chem. Soc., Dalton Trans.* **1980**, 624.

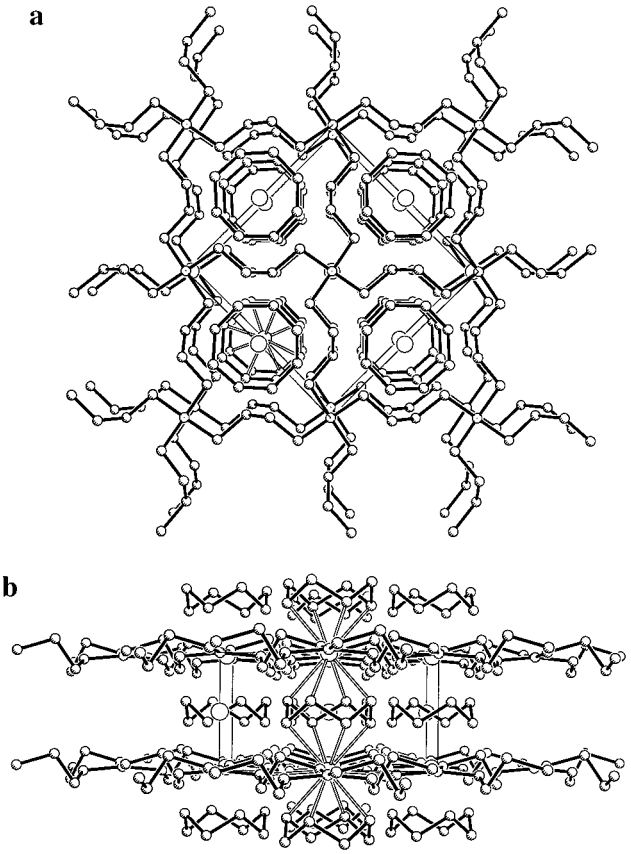

Figure 3. The structure of $Rb_2[Pd(Se_4)_2]\cdot Se_8$ viewed down the (a) [001] and (b) [010] directions. The $[Rb(Se_8)^+]$ chains pass through large Pd_4Se_{16} twenty-membered rectangular rings of the 2D $[Pd(Se_4)_2]^{2-}$ sheet and run along the *c* axis. For one chain the $Rb-Se_{ring}$ interactions are depicted as bonds.

is probably responsible for the slight lengthening of the Se−Se bonds. All secondary Se···Se contacts between the Se_8 rings and the $[Pd(Se_4)_2]^{2-}$ net are longer than 3.28 Å (Table 3).

The complete host−guest structure of $Rb_2[Pd(Se_4)_2]\cdot Se_8$ is presented in Figure 3. The Rb(1) atoms are located within the huge Pd_4Se_{16} 20-membered rings of the sheets whereas the Rb(2) atoms are located within the Se_8 sheets. Rb(1) is coordinated to the crown-like Se_8 rings in a sandwich-like fashion, see Figure 4a. In fact, this coordination scheme forms an infinite $[Rb(Se_8)^+]$ polymeric straight column running along the *c* axis, as depicted in Figure 5a, with the Rb^+ cations lying in the center of the large Pd_4Se_{16} rings (Figure 3). Rb(1) reveals an 8-fold coordination to the ring atoms Se(3) ($4 \times 3.870(1)$ Å) and Se(4) ($4 \times 3.851(1)$ Å). The coordination number of twelve is completed by four additional contacts to Se(1) atoms of the $[Pd(Se_4)_2]^{2-}$ sheets.

Rb(2) is coordinated by four Se_8 rings within the tetragonal plane (Figure 4b), with eight Rb(2)−Se distances of $4 \times 4.085(1)$ Å to Se(3) and $4 \times 4.095(1)$ Å to Se(4). In the *c* direction it has slightly shorter interactions of 4.044(1) Å to four Se(1) atoms of the Se_4^{2-} chains. A remarkable feature is the very short distance of 3.464 Å to two Pd atoms along the *c* axis (Figure 4b, dotted lines), which is significantly shorter than the sum of the covalent radii (3.86 Å). Perhaps this distance represents a small but significant degree of interaction between the electron density of the Pd^{2+} d_z^2 orbital and the empty s orbital of Rb^+.

The stabilization of neutral chalcogenide rings within a host structure is relatively rare. Several compounds reveal isolated molecules or anions with cocrystallized neutral S_8 molecules,

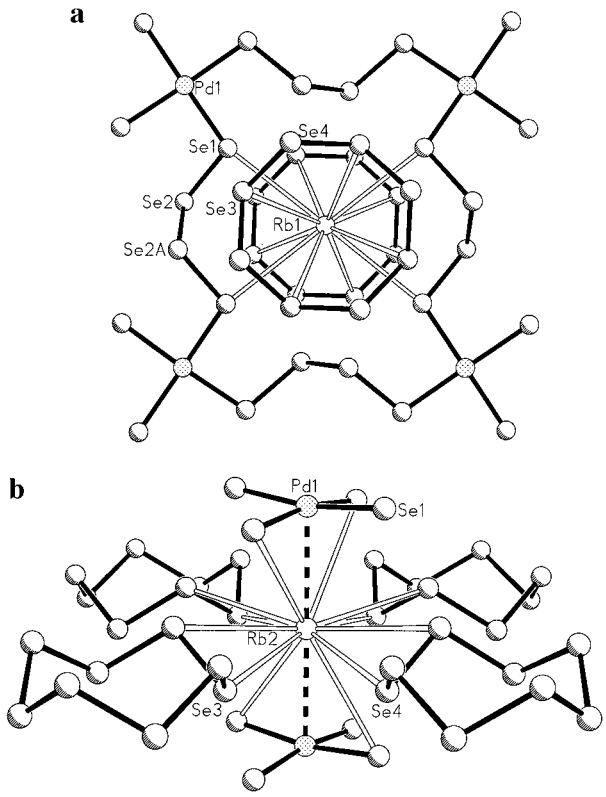

Figure 4. The 12-fold coordination environment of Rb(1) from (a) the [001] direction and (b) the 12-fold coordination of Rb(2) with Rb−Se distances between 4.0440(8) and 4.0946(9) Å; two additional short Rb−Pd distances of 3.4637(4) Å are additionally depicted as dotted bonds.

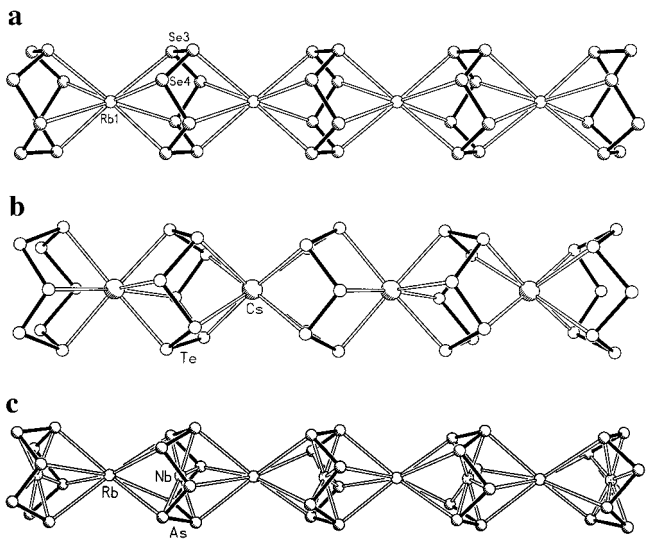

Figure 5. (a) The $[Rb(Se_8)^+]$ chain cation within $Rb_2[Pd(Se_4)_2]\cdot Se_8$, running down the [001] direction in the crystal structure. Similar columns are also present in (b) Cs_4Te_{28}[25] and (c) $[Rb(2,2,2\text{-crypt})]_2[Rb\{NbAs_8\}]$.[29] The alkali metal (and Nb) coordination distances are the following: **I**, Rb−Se 3.8511(9), 3.8704(8) Å; Cs_4Te_{28}, Cs−Te 3.960(2), 3.995(2) Å; $[Rb(2,2,2\text{-crypt})]_2[Rb\{NbAs_8\}]$, Rb−As 3.911(2), 3.930(2) Å, Nb−As 2.615(2), 2.623(2) Å.

among these are $WCl_6\cdot S_8$,[13] $WCl_4S\cdot S_8$,[14] $SnI_4\cdot 2S_8$,[15] $CHI_3\cdot 3S_8$,[16] $SbI_3\cdot 3S_8$,[17] $(Ph_4P)_4[Ag_2S_{20}]\cdot S_8$,[18] and $\{N(PPh_3)_2\}[Ag(S_9)]\cdot S_8$.[19] There are no corresponding examples mentioned in the literature

(13) Cotton, F. A.; Kibala, P. A.; Sandor, R. B. W. *Acta Crystallogr. C* **1989**, *45*, 1287.

(14) Hughes, D. L.; Lane, J. D.; Richards, R. L. *J. Chem. Soc., Dalton Trans.* **1991**, 1627.

for the analogous Se_8 molecule, but other Se_x ($x = 6, 7$) rings are stabilized in $[Na(12\text{-crown-}4)_2^+]_2Se_8^{2-}\cdot(Se_6,Se_7)$[20] and $(Et_4N)_2Se_5\cdot 0.5Se_6\cdot Se_7$.[21] An interesting example where two S_8 molecules act as ligands for an Ag^+ cation was found in $[Ag(S_8)_2]AsF_6$.[22] However, in none of these examples is a crown ether-type interaction observed.

The examples for 2D or 3D host structures with chalcogen rings as guest molecules are even fewer. Interestingly, often they show a stabilization of chalcogenide rings otherwise not known as free species in a possible allotropic structure of the concerned chalcogen.

Neutral S_8 rings are stabilized in $Cs_2Sn_3S_7\cdot 0.5S_8$[23] by embedding them within huge Sn−S rings of the $[Sn_3S_7^{2-}]$ layers. However, in this compound crown ether-like $[Cs(S_8)^+]$ interactions are not seen. Homologous Te_8 rings have been found for the first time in the polytellurides Cs_3Te_{22}[24] and Cs_4Te_{28};[25] in Cs_3Te_{22} they are inserted as double sheets in 2D $[Te_6^{3-}]$ nets, and in Cs_4Te_{28} they are embedded in a 3D $[Te_{20}^{4-}]$ framework. The inclusion in a host structure is responsible for the stabilization of these rings. In these polytellurides the $[Cs(Te_8)^+]$ interactions also seem to play an important role in the formation of the compounds. An unusual large and otherwise unknown Se_{12} ring is stabilized in $(NH_4)_2[Mo_3S_{11.72}Se_{1.28}]_2\cdot Se_{12}$,[26] embedded between sheets of $[Mo_3S_{11.72}Se_{1.28}]^{2-}$ clusters. Te_6 species act as ligands in the interconnection of $[Re_6Te_8]^{2+}$ clusters in $Re_6Te_{16}Cl_6$.[27]

The $[Rb(Se_8)^+]$ columns within the structure of $Rb_2[Pd(Se_4)_2]\cdot Se_8$ (Figure 5a) seem to play an important role in the stabilization of the compound. The linear sandwich-like condensation of two Se_8 molecules is not the only possibility for Rb^+ ions to coordinate chalcogen rings. For comparison, in $Rb_3AsSe_4\cdot 2Se_6$[28] a Rb^+ ion is coordinated to four Se_6 rings in a tetrahedral manner, and the resulting $[Rb(Se_6)_2^+]$ polycation builds a 3D framework with a β-crystobalite-type[9] structure. Therefore, Rb^+ seems to have the adequate diameter to be able to stabilize both Se_6 or Se_8 rings in a linear and tetrahedral coordination manner, respectively. More voluminous Cs^+ ions on the other hand coordinate also in a linear mode with larger Te_8 rings in Cs_3Te_{22}[24] and Cs_4Te_{28}.[25] In fact, the situation in both compounds is very similar to the one given in $Rb_2[Pd(Se_4)_2]\cdot Se_8$. Cs_3Te_{22} reveals sandwich-like $[Cs(Te_8)_2]^+$ species, whereas Cs_4Te_{28} possesses $[Cs(Te_8)^+]$ columns (Figure 5b), also running along the *c* axis of the tetragonal cell and embedded in the tunnels of an anionic 3D tellurium framework $[Te_{20}^{4-}]$. In Cs_3Te_{22} the Cs^+ cation of the $[Cs(Te_8)_2]^+$ lies in the center of a Te_{12} square net, whereas $Rb_2[Pd(Se_4)_2]\cdot Se_8$ exhibits a comparable centering of the Rb^+ cations within the Pd_4Se_{16} 20-membered rings (Figure 4a), suggesting that in both cases the perfect positioning of the alkali metals is jointly responsible for the stability of the structure.

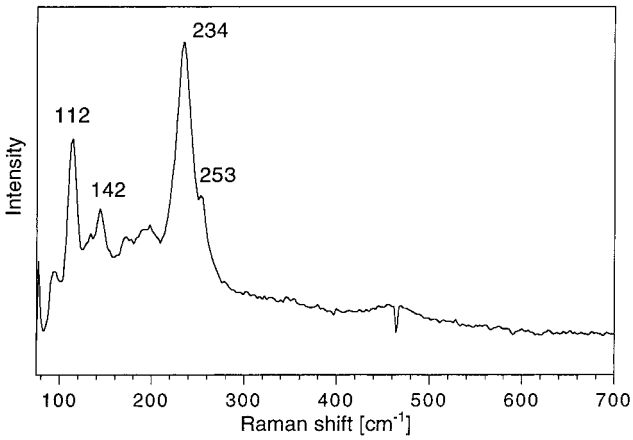

Figure 6. Raman spectrum of $Rb_2[Pd(Se_4)_2]\cdot Se_8$. The bands at 112 and 234 cm^{-1} can be assigned to Se−Se stretches of Se_8 and Se_4^{2-}, respectively.

An interesting isoelectronic and isostructural eight-membered ring species of a Group 15 element was first found in $[Rb(2,2,2\text{-crypt})]_2[Rb\{NbAs_8\}]$.[29] The high charge of the As_8^{8-} ring is partly compensated by a Nb^{5+} cation embedded in the center. A Rb^+ ion coordinates these rings and forms parallel $[Rb(NbAs_8)]^{2-}$ columns, as depicted in Figure 5c. Recently, a similar compound $[K(2,2,2\text{-crypt})]_2[MoAs_8]\cdot en$ was reported[30] through reaction of an en solution of Mo(Me-naphthalene)$_2$ with K_3As_7 in the presence of 2,2,2-cryptand. In this case a free $[MoAs_8]^{2-}$ anion is present, but the electronic structure is very similar to that of the $[NbAs_8]^{3-}$ anion, since in both cases a formally d^0 transition metal is encapsulated within the As_8^{8-} cages. It is also interesting to note that whereas the Rb^+ cations of **I** and the Cs^+ cations of Cs_4Te_{28}[25] possess a strict square prismatic and square antiprismatic coordination, respectively, the situation of the Rb^+ cation in $[Rb(NbAs_8)]^{2-}$ is between these two extremes (Figures 5a−c).

Properties. The Raman spectrum of $Rb_2[Pd(Se_4)_2]\cdot Se_8$ is shown in Figure 6; a broad band with a maximum at 234 cm^{-1} and a second weaker band at 142 cm^{-1} can be assigned to the Se−Se bonds of the Se_4^{2-} chains. This is in good agreement with the Raman spectrum of the trigonal (black) Se form,[31] which shows a strong band at 234 cm^{-1} (with a splitting at 237 cm^{-1}) as well as a weaker band at 141 cm^{-1}. This result is understandable, since the Se_4^{2-} units can be considered as a section of the helical chain of trigonal Se_x. An overtone at ca. 458 cm^{-1} is weaker than in the spectrum of pure trigonal Se_x, but still visible. Additionally, a shoulder at ca. 253 cm^{-1} is identifiable, which is caused by the Se_8 ring molecules. A second strong band at 112 cm^{-1} can also be assigned to the Se−Se stretch of the Se_8 molecules in $Rb_2[Pd(Se_4)_2]\cdot Se_8$. This is in excellent agreement with the reported values for α-monoclinic Se_8.[31] A Pd−Se stretch could not be assigned. The far-IR spectrum in the region 600−130 cm^{-1} shows a strong band at

(15) Laitinen, R.; Steidel, J.; Steudel, R. *Acta Chem. Scand. Ser. A* **1980**, *34*, 687.
(16) Björvatten, T. *Acta Chem. Scand.* **1962**, *16*, 749.
(17) Björvatten, T.; Hassel, O.; Lindheim, A. *Acta Chem. Scand.* **1963**, *17*, 689.
(18) Müller, A.; Römer, R.; Bögge, H.; Kricklmeyer, E.; Baumann, F. W.; Schmitz, E. *Inorg. Chim. Acta* **1984**, *89*, L7.
(19) Müller, A.; Römer, R.; Bögge, H.; Kricklmeyer, E.; Zimmermann, M. *Z. Anorg. Allg. Chem.* **1986**, *534*, 69.
(20) Staffel, R.; Müller, U.; Ahle, A.; Dehnicke, K. *Z. Naturforsch. B* **1991**, *46*, 1287.
(21) Dietz, J.; Müller, U.; Müller, V.; Dehnicke, K. *Z. Naturforsch. B* **1991**, *46*, 1293.
(22) Roesky, H. W.; Thomas, M.; Schrimkowiak, J.; Jones, P. G.; Pinkert, W.; Sheldrick, G. M. *J. Chem. Soc., Chem. Commun.* **1982**, 895.
(23) Marking, G. A.; Kanatzidis, M. G. *Chem. Mater.* **1995**, *7*, 1915.
(24) Sheldrick, W. S.; Wachhold, M. *Angew. Chem., Int. Ed. Engl.* **1995**, *34*, 450.
(25) Sheldrick, W. S.; Wachhold, M. *J. Chem. Soc., Chem. Commun.* **1996**, 607.
(26) Stevens, R. A.; Raymond, C. C.; Dorhout, P. K. *Angew. Chem., Int. Ed. Engl.* **1995**, *34*, 2509.
(27) Mironov, Y. V.; Pell, M. A.; Ibers, J. A. *Angew. Chem., Int. Ed. Engl.* **1996**, *35*, 2854.
(28) Wachhold, M.; Sheldrick, W. S. *Z. Naturforsch. B* **1997**, *52*, 169.
(29) von Schnering, H.-G.; Wolf, J.; Weber, D.; Ramirez, R.; Meyer, T. *Angew. Chem., Int. Ed. Engl.* **1986**, *25*, 353.
(30) Eichhorn, B. W.; Mattamana, S. P.; Gardner, D. R.; Fettinger, J. C. *J. Am. Chem. Soc.* **1998**, *120*, 9708.
(31) Nagata, K.; Ishibashi, K.; Miyamoto, Y. *Jpn. J. Appl. Phys.* **1981**, *20*, 463.

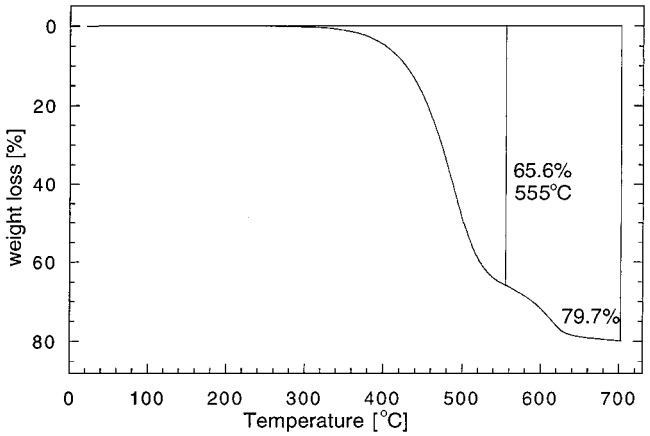

Figure 7. Thermal gravimetric analysis weight-loss diagram of $Rb_2[Pd(Se_4)_2]\cdot Se_8$ under N_2 flow to 700 °C.

142 cm^{-1} and a weaker one at 230 cm^{-1}, which are caused by the Se_4^{2-} chain (literature values for trigonal Se: 145 and 230 cm^{-1}, respectively[31]). A weak band at 258 cm^{-1} could be assigned to the Se_8 ring molecules and is identical to the literature value for α-Se_8.[31]

$Rb_2[Pd(Se_4)_2]\cdot Se_8$ is a semiconductor with an optical band gap at about 1.51 eV. Therefore it agrees well with the values observed for other 2D and 3D Pd polyselenides, which lie within the range of 1.4−1.6 eV, e.g. 1.48 eV for K_2PdSe_{10}.[4]

The thermal stability of $Rb_2[Pd(Se_4)_2]\cdot Se_8$ was examined through thermal gravimetric analysis (TGA) under N_2 flow to 750 °C (Figure 7). The material begins to lose weight at about 280 °C, with a one-step weight loss of about 80% at ca. 700 °C. The examination of the residual turquoise shimmering powder, by X-ray diffraction analysis, showed that its pattern did not match any binary Pd−Se or Rb−Se phase. Comparison with all known ternary systems, however, showed that $Rb_2Pd_3Se_4$[32] was formed. The latter is the only compound that could be assigned from the powder pattern. This interesting monoselenide phase was reported by Bronger et al., and its structure consists of $Pd(Se)_4$ square planes which are connected by common edges to form honeycomb-like 6^3 sheets. Surprisingly, Rb_2PdSe_2[33] is not formed, although the identical Rb:Pd ratio of the starting compound could suggest that its formation might be more likely. Additionally, a weak inflection point at ∼550 °C with a weight loss of ∼66% could be assigned (Figure 7). If the heating process is stopped at this point, the powder pattern of the resulting compound suggests exclusively $Rb_2Pd_3Se_4$, although in this case the pattern is considerably richer in high-angle peaks (Figure 8). In contrast the product obtained at 700 °C has an even stronger (040) peak, indicating the preferable orientation of the honeycomb layers. Other products in the final powders, if present, are either minor phases or amorphous. The selective removal of "Se_8" out of $Rb_2[Pd(Se_4)_2]\cdot Se_8$, leading to a new compound "Rb_2PdSe_8" (presumably isostructural to Cs_2PdSe_8[5]), for which only a theoretical value of 41% weight loss should be expected, does not seem to be possible.

DTA measurements in a closed evacuated quartz ampule show an endothermic peak with a maximum at ca. 241 °C, which can be assigned to the melting point of the compound (Figure 9). This is consistent with the TGA experiment, showing the beginning of weight loss at ∼280 °C. The recrystallization point occurs at ∼191 °C. The X-ray powder pattern of a sample

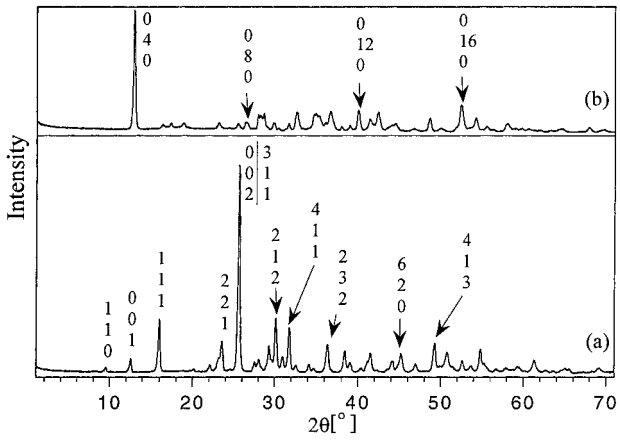

Figure 8. X-ray analysis powder patterns of (a) pure $Rb_2[Pd(Se_4)_2]\cdot Se_8$ at room temperature and (b) after heating to 550 °C, leading to the formation of $Rb_2Pd_3Se_4$.[32] The stronger peaks of $Rb_2[Pd(Se_4)_2]\cdot Se_8$ are indexed; $Rb_2Pd_3Se_4$ shows only a strong (040) peak due to preferential orientation of the phase.

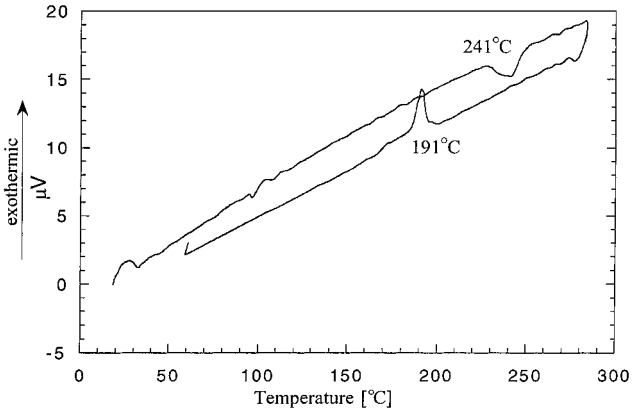

Figure 9. Differential thermal analysis diagram for $Rb_2[Pd(Se_4)_2]\cdot Se_8$ from room temperature to 300 °C; the compound melts at 240 °C and recrystallizes at 191 °C.

heated to 280 °C and then cooled to room temperature shows that $Rb_2[Pd(Se_4)_2]\cdot Se_8$ is still present, but trigonal Se_x is also formed in small amounts as a decomposition product. This clearly shows that the Se_8 rings might be quite stable in the melt, at least for a limited time and at not too high temperatures. By comparison, monoclinic α-Se_8 is only stable up to ca. 155 °C and decomposes before melting, transforming into the stable trigonal modification.[34] Two possible explanations for this remarkable difference in the stability of the Se_8 ring systems can be advanced. Either the host structure of the $[Pd(Se_4)_2]^{2-}$ sheets can behave as a protective "matrix", or the "tight" sandwich crown ether-like coordination of the rings (Figure 5) within the $[Rb(Se_8)^+]$ chains can lead to their higher stability. The ionic Rb···Se interactions should still be very strong in the liquid state, circumventing a fast ring opening polymerization at low temperatures.

During a second heating/cooling cycle to 280 °C an additional endothermic peak at about 220 °C appears, which could easily be assigned to the melting point of trigonal selenium. Additional cycles lead to more and more elemental selenium. $Rb_2[Pd(Se_4)_2]\cdot Se_8$ shows no other phase transition up to 600 °C. A similar heating/cooling cycle to 400 °C leads only to $PdSe_2$ as a decomposition product. The polymerization of the Se_8 rings in the melt at higher temperatures might initiate the decomposition process of $Rb_2[Pd(Se_4)_2]\cdot Se_8$.

(32) Bronger, W.; Rennau, R.; Schmitz, D. *Z. Anorg. Allg. Chem.* **1991**, *597*, 27.

(33) Bronger, W.; Jäger, S.; Rennau, R.; Schmitz, D. *J. Less-Common Met.* **1989**, *154*, 261.

(34) Hollemann, A. F.; Wiberg, N.; Wiberg, E. *Lehrbuch der Anorganischen Chemie*, 101st ed.; deGruyter: Berlin, 1995; pp 613−619.

The consideration of both the TGA and DTA results gives some interesting conclusions about the thermal behavior of $Rb_2[Pd(Se_4)_2]\cdot Se_8$. Under the dynamic conditions of the TGA experiment, after melting of the compound, the N_2 flow is responsible for the removal of selenium, which causes decomposition of the Pd polyselenide to $Rb_2Pd_3Se_4$. However, in a closed system (DTA), the building blocks (Se_8, Se_4^{2-}) can survive by staying in the melt (in a limited temperature range) and rebuild the structure of $Rb_2[Pd(Se_4)_2]\cdot Se_8$ on cooling.

Conclusion

The new synthesized compound $Rb_2[Pd(Se_4)_2]\cdot Se_8$ has a unique two-dimensional structure composed of alternating sheets of $[Pd(Se_4)_2]^{2-}$ nets and neutral Se_8 rings in a crown conformation. Its structure differs significantly from its "neighboring" alkali metal Pd polyselenides, K_2PdSe_{10}[4] and Cs_2PdSe_8,[5] which both have a 3D structure of two interpenetrating frameworks.

The stability of $Rb_2[Pd(Se_4)_2]\cdot Se_8$ in both the solid and liquid state is remarkable. On one hand in the liquid state the building blocks of the structure can survive and rebuilt the compound upon crystallization. The removal of the Se_8 rings on the other hand leads to a collapse of the structure with the formation of the ternary phase $Rb_2Pd_3Se_4$[32] as a decomposition product. The $[Rb(Se_8)^+]$ columns seem to play a key role in the stabilization of the compound.

It is still not clear if a Pd polyselenide with a three-dimensional buildup, similar to those of K_2PdSe_{10} or Cs_2PdSe_8, is also possible with Rb^+ under modified conditions. Does it really make that much difference in the phase stability in going from Cs_2PdSe_8 to Rb_2PdSe_8 or from K_2PdSe_{10} to Rb_2PdSe_{10}? Perhaps not, however, the pieces in $Rb_2[Pd(Se_4)_2]\cdot Se_8$ fit so remarkably well together that it is conceivable that the stability of Rb_2PdSe_8 or Rb_2PdSe_{10} is undermined in favor of the Se_8 encapsulating compound. Since so far $Rb_2[Pd(Se_4)_2]\cdot Se_8$ is always formed in at least fair yields even under a greater variation of the stoichiometric ratio of the reactants (see Experimental Section), it is obvious that it represents a very stable structure type. One explanation for this could be the early formation of Se_8 crown-like rings in the melt, favored as good coordinating species for the Rb^+ cations. It is possible that the Se_8−alkali metal coordination is optimum for Rb^+. Initially formed sandwich molecules, $[Rb(Se_8)_2]^+$, for example, can subsequently favor the formation of **I** over "Rb_2PdSe_8" or "Rb_2PdSe_{10}". Further investigations of various reactant systems Rb−Pd−Se with the aim to isolate a three-dimensional Rb polyselenide are in progress. $Rb_2[Pd(Se_4)_2]\cdot Se_8$ is exemplary for demonstrating that the Pd^{2+}/Se_x^{2-} polyselenide system is able to react with a variety of offered cations by forming an appropriate polyselenide framework to build a stable compound.

Experimental Section

Reagents. Chemicals were used as obtained without further purification: $PdCl_2$ powder, Lancaster; Se powder 100 mesh, Aldrich; methanol 99.9%, J. T. Baker; diethyl ether >99.0%, CCI. Na_2Se was prepared by dissolving stoichiometric amounts of sodium metal and elemental selenium in liquid ammonia.

Synthesis. All experiments and manipulations were performed under an atmosphere of dry nitrogen with a vacuum atmosphere Dri-Lab glovebox.

$Rb_2[Pd(Se_4)_2]\cdot Se_8$ was first prepared by a reaction of Rb_2CO_3 (0.046 g, 0.2 mmol), $PdCl_2$ (0.036 g, 0.2 mmol), Na_2Se (0.030 g, 0.25 mmol), and Se (0.040 g, 0.5 mmol) in MeOH (0.5 mL). The chemicals were mixed together and charged into a Pyrex tube (∅ 13 mm, wall thickness 1.6 mm), which was sealed under vacuum and heated at 150 °C for 36 h. Black, shiny rectangular crystals and a small amount of black powder were isolated by filtration and washed with acetone and water several times.

Semiquantitative analysis by SEM/EDS technique on single crystals showed a Rb:Pd:Se ratio of 2.1:1:15.8 (average of three crystals). No significant sodium content could be detected in these analyses. EDS of a bigger sample area gave averaged higher values for Pd and Se ("$Rb_{1.1}PdSe_{21}$"). The purity of the compound was confirmed by comparison of the powder X-ray diffraction pattern of the homogenized and ground material with the one calculated from single-crystal X-ray data.[35] Only slight impurities of elemental selenium were present besides the main product Rb_2PdSe_{16}. To optimize the synthesis by using the reactants in a stoichiometric ratio, Rb_2CO_3 (0.046 g, 0.2 mmol), $PdCl_2$ (0.036 g, 0.2 mmol), Na_2Se (0.050 g, 0.4 mmol), and Se (0.224 g, 2.8 mmol) were reacted in MeOH (0.5 mL) for 48 h at 140 °C. This resulted, according to the powder pattern, in a quantitative synthesis of $Rb_2[Pd(Se_4)_2]\cdot Se_8$ without any impurities.

Physicochemical Methods. Solid-State UV/Vis Spectroscopy. UV−vis−near-IR diffuse reflectance spectra were obtained at room temperature on a Shimadzu UV-3101PC double-beam, double-monochromator spectrophotometer in the wavelength range of 200−2500 nm. $BaSO_4$ powder was used as a reference (100% reflectance) and base material, on which the ground powder sample was coated. Reflectance data were converted to absorbance data as described elsewhere.[36] The band gap energy value was determined by extrapolation from the linear portion of the absorption edge in a (α/S) versus E plot.

Thermal Gravimetric Analysis (TGA). TGA analysis was performed on a computer-controlled Shimadzu TGA-50 thermal analyzer. Thirteen milligrams of the sample was charged into a quartz bucket and heated to 700 °C at a rate of 5 °C/min under a steady flow of dry N_2 gas. The residue was examined by X-ray powder diffraction.

Differential Thermal Analysis (DTA). DTA experiments were performed on a computer-controlled Shimadzu DTA-50 thermal analyzer. Fifteen to twenty milligrams of ground material was sealed in a carbon-coated quartz ampule under vacuum. A sealed quartz ampule of equal mass filled with Al_2O_3 was used as a reference. The sample was heated to the desired temperature at 5 °C/min and isothermed for 5 min, followed by cooling at −5 °C/min to 50 °C. The sample stability was monitored by running multiple heating/cooling cycles. The residues were examined by X-ray powder diffraction.

Raman Spectroscopy. Raman spectra of suitable crystals with a clean surface were recorded on a Holoprobe Raman spectrograph equipped with a 633 nm Helium−Neon laser and a CCD camera detector. The instrument was coupled to an Olympus BX60 microscope. The spot size of the laser beam was 10 μm when a 50× objective lens was used.

Infrared Spectroscopy. Infrared spectra in the far-IR region (600−100 cm^{-1}) were recorded on a computer-controlled Nicolet 750 Magna-IR Series II spectrometer equipped with a TGS/PE detector and a silicon beam splitter in 4 cm^{-1} resolution. The samples were mixed with ground dry CsI and pressed into translucent pellets.

Semiquantitative Microprobe Analysis. The analyses were performed with use of a JEOL JSM-35C scanning electron microscope (SEM) equipped with a Tracor Northern energy dispersive spectroscopy (EDS) detector. Data were acquired on several crystals with use of an accelerating voltage of 20 kV and 35 s accumulation time.

X-ray Crystallography. A single crystal of $Rb_2[Pd(Se_4)_2]\cdot Se_8$ with dimensions 0.10 × 0.05 × 0.03 mm was sealed in a glass capillary (∅ 0.3 mm, wall thickness 1/100 mm) and mounted on a goniometer head. Crystallographic data were collected at 295 K on a Siemens Platform CCD diffractometer using graphite monochromatized Mo Kα radiation. The data were collected over a full sphere of reciprocal space, up to 57.1° in 2θ (completeness 97.0%). The individual frames were measured with an ω rotation of 0.3° and an acquisition time of 30 s. The SMART[37] software was used for the data acquisition and SAINT[38]

(35) CERIUS^2, Version 2.35; Molecular Simulations Inc.: Cambridge, U.K., 1995.

(36) Zhang, X.; Kanatzidis, M. G. *J. Am. Chem. Soc.* **1994**, *116*, 1890.

(37) SMART, Version 5: Siemens Analytical X-ray Systems, Inc.: Madison, WI, 1998.

Table 1. Crystal Data and Structure Refinement for $Rb_2[Pd(Se_4)_2]\cdot Se_8$

empirical formula	Rb_2PdSe_{16}
formula weight	1540.72
temp (K)	298
radiation, wavelength (Å)	Mo Kα, $\lambda = 0.71073$
crystal system	tetragonal
space group	$P\bar{4}b2$ (No. 117)
a (Å)	12.6748(8)
c (Å)	6.9273(7)
V (Å^3)	1112.8(2)
Z	2
ρ_{calc} (g cm^{-3})	4.598
μ(Mo Kα) (mm^{-1})	31.328
F(000)	1328
crystal size (mm)	0.10 × 0.05 × 0.03
crystal shape, color	rectangular rod, black
θ range (deg)	1.61−28.55
completeness to $\theta = 28.55°$	97.0%
index ranges	$-16 \le h \le 16$, $-16 \le k \le 16$, $-9 \le l \le 9$
no. of data collected	13102
no. of unique data	1374 ($R_{int} = 0.0596$)
no. reflections $F_o > 4\sigma(F_o)$	1201
max and min transmission	0.4533 and 0.1457
refinement method	full-matrix least-squares on F^2
data/restraints/parameters	1374/0/45
goodness-of-fit on F^2	1.376
final R indices [$I > 2\sigma(I)$]	$R_1 = 0.0258$, $wR_2 = 0.0449$
R indices (all data)	$R_1 = 0.0336$, $wR_2 = 0.0455$
absolute structure Flack parameter	0.00(4)
largest diff peak/hole (e·Å^{-3})	0.597 and −1.283

Table 2. Atomic Coordinates and Equivalent Isotropic Displacement Parameters (Å^2 × 10^3) for $Rb_2[Pd(Se_4)_2]\cdot Se_8$

	x	y	z	U_{eq}[a]
Rb(1)	0.5	0	0	66(1)
Rb(2)	0	0	0.5	80(1)
Pd(1)	0	0	0	15(1)
Se(1)	0.8121(1)	0.0356(1)	0.9674(1)	27(1)
Se(2)	0.7871(1)	0.7975(1)	0.1302(1)	32(1)
Se(3)	0.9196(1)	0.6919(1)	0.5911(1)	29(1)
Se(4)	0.6904(1)	0.9222(1)	0.5908(1)	30(1)

[a] The equivalent displacement factor is defined as one third of the trace of the orthogonalized U^{ij} tensor.

for the data extraction and reduction. The absorption correction was performed with SADABS.[39] The complete data collection parameters and details of the structure solution and refinement for the compound are given in Table 1. All atoms in the structure were refined anisotropically. Fractional atomic coordinates and equivalent isotropic displacement parameters (U_{eq}) are given in Table 2, bond parameters in Table 3.

Structure solution and refinements were performed with the SHELXTL package of crystallographic programs.[40] Systematic absence conditions of the data set gave three possible tetragonal space groups, centrosymmetric $P4/mbm$ (No. 127) and noncentrosymmetric $P\bar{4}b2$ (No. 117) and $P4bm$ (No. 100). $|E^2 - 1|$ statistics were ambiguous regarding a center of symmetry. All three space groups were tried and only the noncentrosymmetrical space group $P\bar{4}b2$ gave a crystallographically reasonable result. The possibility of a missing center of symmetry was examined with the program MISSYM,[41] but no indications were found. The structure was refined in $P\bar{4}b2$ to $R_1 = 2.58\%$ and $wR_2 = 4.49\%$ for 1201 data with $I > 2\sigma$ and $R_1 = 3.36\%$ and $wR_2 = 4.55\%$ for all 13102 data. The Flack absolute structure parameter was refined to 0.00(4) with a racemic ratio of 86.6:13.3%.

Table 3. Bond Lengths (Å) and Angles (deg) for $Rb_2[Pd(Se_4)_2]\cdot Se_8$

		$[Pd(Se_4)_2]^{2-}$	
bond lengths		angles	
Pd(1)−Se(1)	2.4339(6)	Se(1)−Pd(1)−Se(1)	90.495(3)
Se(1)−Se(2)	2.354(1)	Se(1)−Pd(1)−Se(1)	169.34(3)
Se(2)−Se(2)	2.357(1)	Se(2)−Se(1)−Pd(1)	106.31(3)
		Se(1)−Se(2)−Se(2)	104.52(3)
		torsion angle Se_4^{2-}	
		Se(1)−Se(2)−Se(2)−Se(1)	100.5
		Se_8 ring	
bond lengths		angles	
Se(3)−Se(3)	2.364(2)	Se(3)−Se(3)−Se(4)	102.56(3)
Se(3)−Se(4)	2.3676(9)	Se(3)−Se(4)−Se(4)	103.40(4)
Se(4)−Se(4)	2.379(2)	torsion angles	
		Se(3)−Se(3)−Se(4)−Se(4)	104.1
		Se(4)−Se(3)−Se(3)−Se(4)	103.5
		Se(3)−Se(4)−Se(4)−Se(3)	104.9

Long Contacts $[Pd(Se_4)_2]^{2-}\cdots Se_8$ (Å)

Se(2)···Se(4)	3.287	Se(1)···Se(4)	3.354
Se(2)···Se(3)	3.372	Se(1)···Se(3)	3.465

Coordination distances of Rb(1) and Rb(2) (Å)[a]

Rb(1)−Se(4)	3.8511(9)	Rb(2)−Pd(1)#8	3.4636(4)
Rb(1)−Se(4)#1	3.8511(9)	Rb(2)−Pd(1)	3.4637(4)
Rb(1)−Se(4)#2	3.8511(9)	Rb(2)−Se(1)#9	4.0440(8)
Rb(1)−Se(4)#3	3.8512(9)	Rb(2)−Se(1)#8	4.0440(8)
Rb(1)−Se(3)#4	3.8704(8)	Rb(2)−Se(1)#10	4.0440(7)
Rb(1)−Se(3)#5	3.8704(8)	Rb(2)−Se(1)#4	4.0440(7)
Rb(1)−Se(3)#6	3.8705(8)	Rb(2)−Se(3)#9	4.0848(8)
Rb(1)−Se(3)#7	3.8705(8)	Rb(2)−Se(3)#8	4.0848(8)
Rb(1)−Se(1)#1	3.9885(7)	Rb(2)−Se(3)#4	4.0848(8)
Rb(1)−Se(1)#2	3.9885(7)	Rb(2)−Se(3)#10	4.0848(8)
Rb(1)−Se(1)#3	3.9885(7)	Rb(2)−Se(4)#9	4.0946(9)
Rb(1)−Se(1)	3.9885(7)	Rb(2)−Se(4)#8	4.0946(9)
		Rb(2)−Se(4)#10	4.0946(8)
		Rb(2)−Se(4)#4	4.0946(9)

[a] Symmetry transformations used to generate equivalent atoms: #1 $y - 1/2, x + 1/2, -z + 2$; #2 $-y + 3/2, -x + 3/2, -z + 2$; #3 $-x + 1, -y + 2, z$; #4 $y, -x + 2, -z + 2$; #5 $-y + 1, x, -z + 2$; #6 $x - 1/2, -y + 3/2, z$; #7 $-x + 3/2, y + 1/2, z$; #8 $x, y, z + 1$; #9 $-x + 2, -y + 2, z + 1$; #10 $-y + 2, x, -z + 2$.

Acknowledgment. Support from the National Science Foundation (CHE 96-33798, Chemistry Research Group) and the Petroleum Research Fund, administered by the American Chemical Society, is gratefully acknowledged. We acknowledge the use of the W.M. Keck Microfabrication Facility at Michigan State University, a NSF MRSEC facility. Part of this work was carried out using the facilities of the Center for Electron Optics of Michigan State University. M.W. thanks the Deutsche Forschungsgemeinschaft for a postdoctoral research fellowship.

Supporting Information Available: Tables of positional and thermal anisotropic thermal parameters of all atoms, bond distances and angles for **I** (PDF). This material is available free of charge via the Internet at http://pubs.acs.org.

JA984053G

(38) SAINT, Version 4: Siemens Analytical X-ray Systems, Inc.: Madison, WI, 1994−1996.

(39) SADABS: Sheldrick, G. M. University of Göttingen, Germany.

(40) Sheldrick, G. M.; SHELXTL, Version 5.1, Siemens Analytical X-ray Systems, Inc.: Madison, WI, 1997.

(41) MISSYM: (a) LePage, Y. *J. Appl. Crystallogr.* **1987**, *20*, 264. (b) LePage, Y. *J. Appl. Crystallogr.* **1988**. *21*, 983.